Visualized-experimental investigation on the melting performance of PCM in 3D printed metal foam

Zhijie Zhou[a], Zhuohuan Hu[a,*], Dan Wang[a], Hongwei Wu[a,b]

[a]School of Energy and Power Engineering, University of Shanghai for Science and Technology, 200093, Shanghai, China.
[b]School of Physics, Engineering and Computer Science, University of Hertfordshire, Hatfield, AL10 9AB, UK.

*Corresponding Author (Zhuohuan Hu): Email: huzhuohuan@hotmail.com

ABSTRACT

In this article, a new composite phase change material (PCM) with metal foam based on three-dimensional (3D) printed technology has been proposed to reduce the structural parameter uncertainties of metal foam. The composite PCM melting performance was visualized systematically, while both the phase and temperature fields were obtained using photographic and infrared technology. The temperature variations of PCM at different distances from the heating surface on the same level as the internal wall were also captured. Experimental results indicated that: (i) the melting rate of the composite PCM could be significantly improved by 2.5 times when adding 3D printed ALSI10MG aluminium alloy metal foam with a porosity of 0.838; (ii) the phase change interface (PCI) and the temperature contour is similar to that of the metal foam frame; (iii) the enhancement of heat conduction of metal foam is greater than its hindrance to natural convection in composite PCM; (iv) the contact thermal resistance perpendicular to the heat transfer direction could slow down the phase change rate; (v) local thermal non-equilibrium exists between the 3D printed metal foam and PCM. The metal foam fabricated by 3D printed technology has the ability of enhance the heat transfer and the phase change for composite PCM.

KEY WORDS: Phase change material, 3D printed, visualization, melting

1. INTRODUCTION

The introduction of carbon neutrality stimulates extensive research into the efficient utilization and storage of energy. Energy storage technology can effectively solve the contradiction between energy supply and demand in time and space. Among the energy storage technologies, phase change thermal storage has attracted wide attention due to its excellent advantages including large latent heat and almost constant temperature during charging/discharging processes. However, the low thermal conductivity of phase change material (PCM) greatly limits its effective absorption and release of thermal energy. To overcome this limitation, great effort has been devoted to improving the thermal conductivity of PCM. In general, two typical methods are normally used to improve the thermal conductivity of PCM, they are: (1) complexity of PCM with solid media, such as fins [1-2] or metal foam [3-4]. (2) enhancement with nanoparticles [5-6], or carbon fibers [7-8] dispersed into the PCM. According to [1-8], the metal foam has distinctive characteristics of high thermal conductivity, large specific surface area, strong structural interconnection and a good fluid mixing effect, which could be used as a good candidate for improving the performance of PCM [9].

Many researchers have extensively investigated the internal heat transfer process of composite PCM (metal foam/PCM composite). Yao et al. [9-10] explored the phase change process of the composite PCM through a visualized-experimental approach. It was found that the fundamental problems such as the local evolution of the phase change interface (PCI), the influence of the volume change of the paraffin, the thermal response characteristics, and the local thermal non-equilibrium effect can be

more intuitively observed. Li et al. [11] compared the phase change process of the nano-encapsulated PCM (NEPCM) and the metal foam/NEPCM composite through visualization. Their results showed that the phase change speed of the nano-encapsulated PCM could be greatly improved when adding metal foam. Feng et al. [12] conducted an experimental study on the solidification process of composite PCM at different porosity and pores per inch (PPI). Their results demonstrated that the metal foam could increase the freezing rate of the PCM, but the PPI of the metal foam showed little effect on the freezing rate since heat conduction played a dominant role in the solidification process. Mancin et al. [13] experimentally proved that the embedding of metal foam could effectively increase the phase change speed of the PCM. It was also observed that the temperature distribution of the composite PCM is more uniform. Tian et al. [14] carried out an experimental study to investigate the phase change performance of the composite PCM under different tilt angles. The PCI changes were captured by a high-definition (HD) camera. Their results proved that the tilt angle showed little effect on the temperature uniformity of composite PCM. Caliano et al. [15] conducted an experimental study and proved that the natural convection during the solidification process could be ignored and the entire heat transfer process could be dominated by the heat conduction. However, natural convection played a major role in the melting process. Siahpush et al. [16] experimentally investigated the melting and solidification process of both pure PCM and composite PCM. Their results demonstrated that, compared with pure PCM, the solidification and melting times of composite PCM decreased 290 min and 250 min when copper porous foam with a porosity of 95% was applied. Diani et al. [17] observed the melting process of the composite PCM and the pure PCM using an HD camera. Their experimental results stated that the metal foam can effectively improve the melting rate of the PCM.

On the numerical side, many research works have already been investigated on the phase transition process of composite PCM using microscopic approaches. Hu et al [18] established a 3D numerical model of composite PCM and calculated the melting process of pure PCM and composite PCM. Their results illustrated that the effective thermal conductivities of composite PCMs with 70% and 95% porosities aluminum foams can be enhanced about 123 and 17 times compared with that of pure PCM. Yang et al. [19] carried out a pore-scale numerical investigation to study the phase transition process of composite PCM and found that natural convection could play an important role in the melting process. Zhang et al. [20] and Hu et al. [21] conducted a 3D numerical study and found that the gradient arrangement of the metal foam could further improve its heat transfer performance. Li et al. [22] performed a Lattice Boltzmann model (LBM) simulation to investigate the composite PCM with the gradient metal foam. Their results demonstrated that the gradient-arranged metal foam could effectively solve the "dead zone" problem in the middle and late stages of melting. Feng et al. [23] conducted a pore-scale numerical simulation on the phase change heat transfer process of the composite PCM. They observed that the heat transfer performance of the composite PCM could be further enhanced by combining the composite PCM with fins.

It is noted that the flexibility of 3D printed technology can make the fabrication of tiny porous media possible [24]. Jafari et al. [25] examined the heat transfer performance of the porous structure fabricated by the selective laser melting (SLM). Their results proved the heat pipes in conjunction with a 3D-printed wick could significantly improve the heat transfer performance. Ramirez et al. [26] designed Cu reticulated mesh and stochastic open cellular foams using 3D printed technology. These open cell structural components can demonstrate considerable potential in complex thermal management systems. Fratalocchi et al. [27] printed periodic open cell structures using AlSi7Mg0.63D, which enhanced the heat transfer performance of the fixed-bed Fischer-Tropsch process by improving the radial thermal conductivity and contact between the support and the reactor wall. Ryan et al. [28] proposed the porous titanium scaffold made by 3D printed technology in orthopedic applications. For material properties of 3D printed porous metal materials, Li et al. [29] and Sing et al. [30] investigated the effect of mesh structure and process parameters on the material mechanical properties for 3D printed mesh metals, respectively.

Although many significant results have been obtained in demonstrating the enhancement effect of traditional metal foam on the phase transition process of PCM. This paper applies the SLM technique to produce structurally controlled metal foams. The complex melting phenomena were visualized from the top and front views in melting processes with cameras and an infrared camera. Thermocouples were also employed to obtain internal local temperature variations. Furthermore, the enhancement effect of 3D printed metal foam on heat transfer and the effect on natural convection was investigated. Finally, the influence of contact thermal resistance on heat transfer performance in different directions was studied.

2. EXPERIMENTAL METHOD

2.1. Experimental apparatus

Fig. 1 shows the schematic design of the experimental setup. The shells of the cases were constructed by plexiglasses with a thickness of 3 mm, and the internal volume is 20 mm × 20 mm × 12 mm. The fiberglass was added to three sides for heat preservation except for wall D. During the test, the Omega T-type (TC#1) thermocouple was applied to measure the temperature variation of heating wall A. The Omega T-type (TC#2, TC#3, TC#4, and TC#5) thermocouples were adopted to measure the local temperature and placed at the same height of 9 mm on wall B. The detailed positions of thermocouples are shown in Fig. 1. The Agilent 34972A data acquisition system was utilized to record data for analysis. The temperature distributions from the top view were captured by a FLIR A600 infrared camera, while the top and front phase fields were captured by cameras.
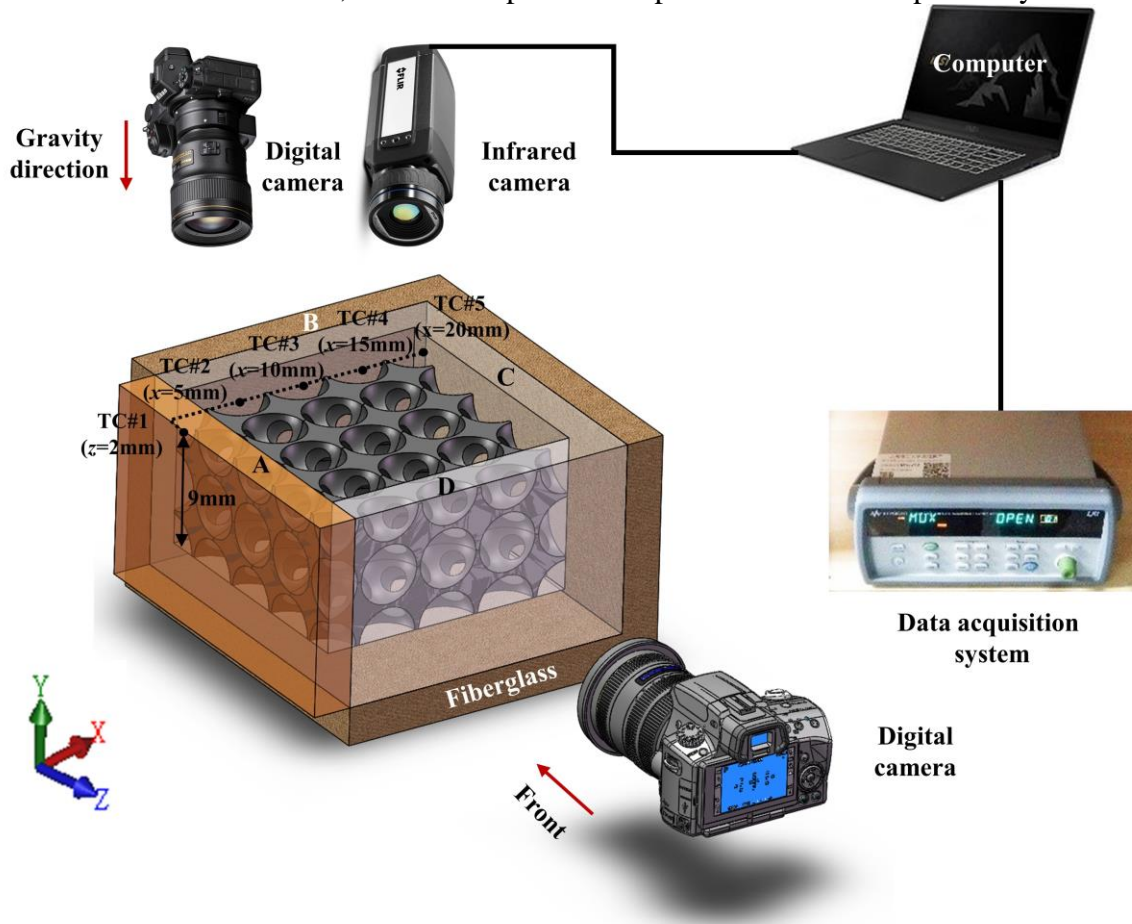

Fig. 1. Experimental apparatus.

3

To explore the effect of the contact thermal resistance between the metal foams on the melting process of composite PCM, two different arrangements (case 1 and case 2) were set up, as shown in Fig. 2. For case 1, all metal foams were placed perpendicular to wall A, i.e. the contact thermal resistances were parallel to the heating direction. While for case 2, the metal foams were parallel to wall A, i.e. the contact thermal resistances were perpendicular to the heating direction. In Fig. 2, the black dotted lines indicated the contact thermal resistance position.

Prior to running the test, the melted paraffin was first poured into the container until it filled the entire experimental space. Then pure PCM, case 1 and case 2 were cooled to the ambient temperature that was controlled to be 26 °C. The temperature of wall A was adjusted to 70 °C, and at the same time, digital cameras, infrared camera and data acquisition systems were activated.
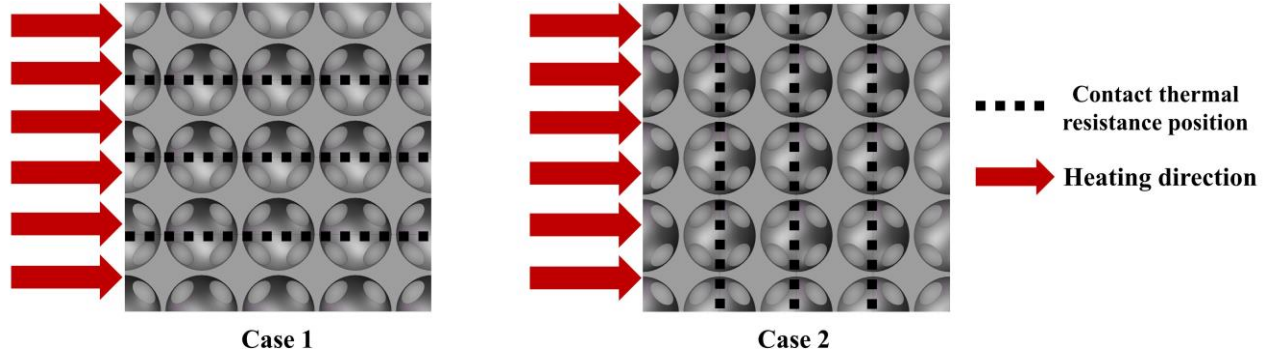

Fig. 2. Two different arrangements from the top view:
case 1- contact thermal resistance position is parallel to the heating direction; case 2 - contact thermal resistance position is perpendicular to the heating direction.

2.2. PCM and 3D printed metal foam

In the current work, paraffin supplied by RT42 (Rubitherm) is selected as PCM and the metal material is ALSI10MG aluminum alloy. The Thermophysical properties of ALSI10MG aluminum alloy, RT42 and plexiglass are listed in Table 1. Table 2 lists the technical parameters of the 3D printer machine (HBD-80). The heat transfer performance of composite PCM mainly depends on the structural parameters of the metal foam, such as pore size, porosity, material, and effective thermal conductivity. However, the metal foam fabricated by conventional methods, such as powder sintering, powder casting and deposition method, is normally to produce random internal structure. As a newly developed technology in metal 3D printed, SLM technology has large geometric freedom. With this technology, manufacturers can directly create free-form foam structures with complex geometric shapes and optimized internal pore structures without other limitations and constraints of processing methods. The geometric size and shape of the metal foam could be controlled by 3D printed technology, and the randomness of the internal structure could also be eliminated [31].

Table 1 Thermophysical properties of ALSI10MG aluminum alloy[32], RT42[33] and plexiglass.

Thermophysical properties	ALSI10MG aluminum alloy	RT42	plexiglass
Melting temperature, $T_m \left({}^{\circ}\mathrm{C} \right)$	—	42	—
Latent heat, $L \left(\mathrm{KJ\ kg^{-1}} \right)$	—	165	—
Thermal conductivity, $\lambda \left(\mathrm{W\ m^{-1}\ K^{-1}} \right)$	175	0.2	0.19
Specific heat, $C_p \left(\mathrm{J\ kg^{-1}\ K^{-1}} \right)$	900	2000	1464

Density, ρ (kg m^{-3}) (solid/liquid)	2670/—	880/760	1180/—
Dynamic viscosity, μ (Pa s)	—	2.35×10^{-2}	—
Thermal expansion coefficient, β (K^{-1})	—	1×10^{-3}	—

Table 2 Technical parameters of the 3D printer (HBD-80)

Item	Value
Laser power	200 W
Linear Scanning speed	≤10000 mm/s
Layer thickness	10 μm-40 μm
Layer focus diameter	40 μm-80 μm

Fig. 3 displays the manufacturing process of the geometric model [21]. The metal foam is made by cutting a ball of diameter b in the center and 8 corners of a cube with side length a. The porosity is defined as the percentage of the porous volume to the total volume of the cube, and can be obtained using Eq. (1).

$$\varepsilon = 1 - \frac{V_s}{V_{tot}} \tag{1}$$

where ε is the porosity, V_s is the volume of the metal foam frame, and V_{tot} is the total volume of the cube. In the current test, the porosity of the model is 0.838 and the side length between the cubes is a=5 mm. The diameter of the cube is b=4.7 mm and the distance from the center ball to the vertex ball is c=4.3 mm. A metal foam model and metal foam sample are shown in Fig. 4 (a) and (b). The metal foam sample was assembled in the shell structure, as illustrated in Fig. 5.
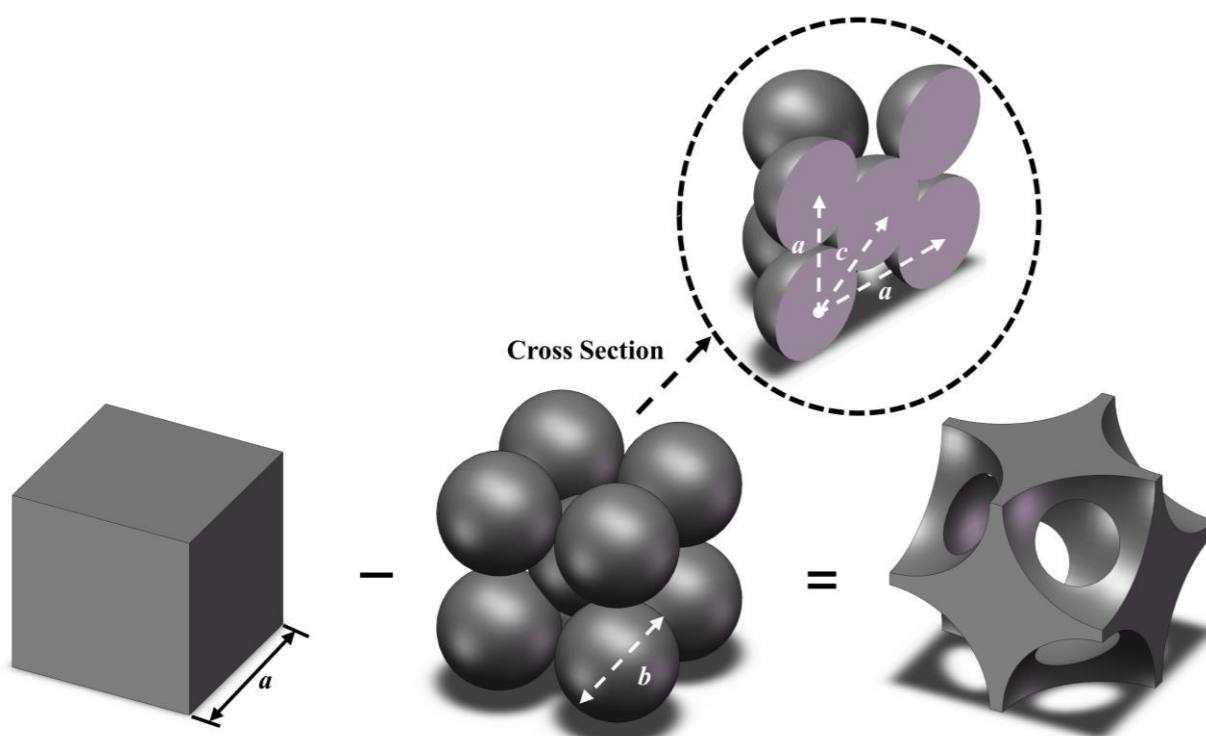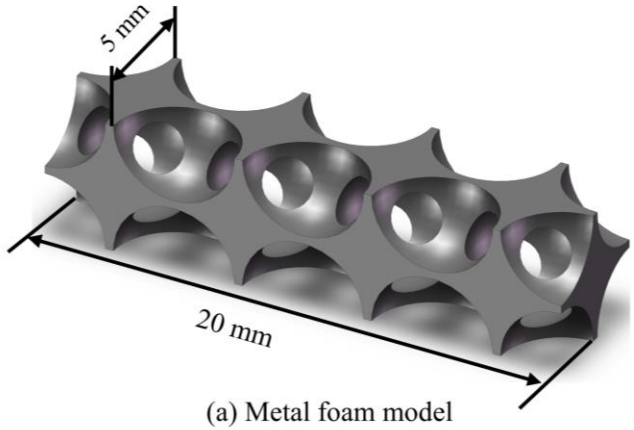

Fig. 3. Schematic diagram of the geometry creation.

(a) Metal foam model

(b) Metal foam sample

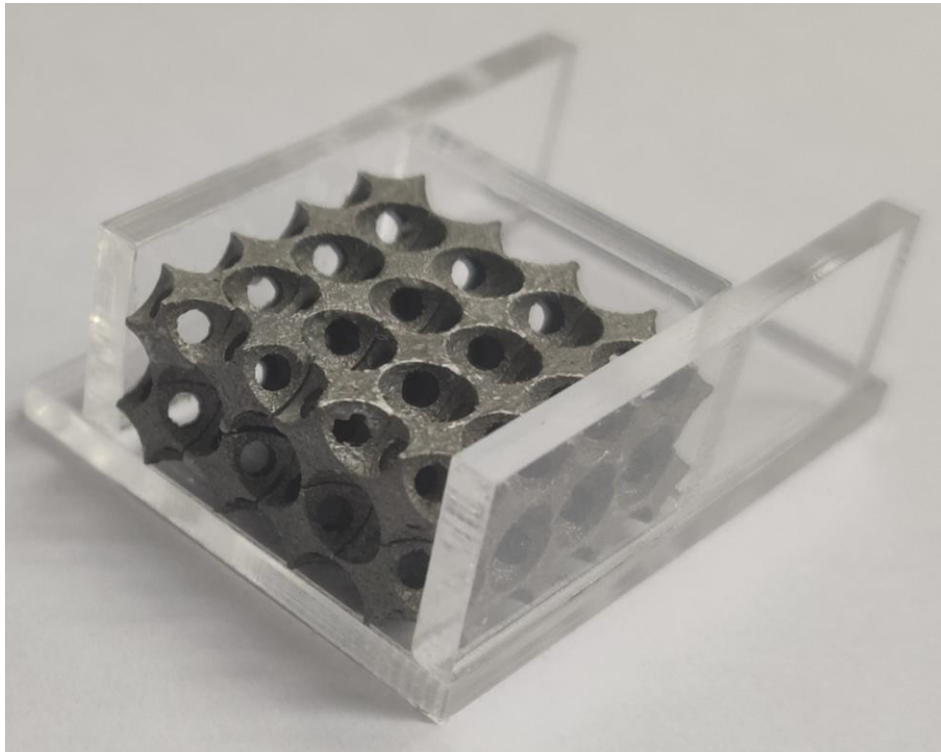**Fig. 4.** 3D printed aluminum alloy metal foam.

Fig. 5. Shell structure.

2.3. Governing equations

During the melting process, the solid PCM absorbs the heat and melts afterwards. In the current study, the fluid flow of the molten PCM is assumed to be Newtonian, in-compressible, and laminar. The physical properties, except for the density, of the metal and PCM are independent of temperature. Based on the above assumptions, the governing equations for the melting process of composite PCM could be given by as follows [19]:

$$\nabla \cdot \vec{u} = 0 \tag{2}$$

$$\rho_{\mathrm{f}} \frac{\partial \vec{u}}{\partial t} + \rho_{\mathrm{f}} \left(\rho_{\mathrm{f}} \cdot \nabla \right) \vec{u} = -\nabla P + \mu_{\mathrm{f}} \nabla^2 \vec{u} + A\vec{u} + \rho_{\mathrm{f}} \vec{g} \beta \left(T_{\mathrm{f}} - T_{\mathrm{m}} \right) \tag{3}$$

$$\rho_{\mathrm{f}} c_{p,\mathrm{f}} \frac{\partial T_{\mathrm{f}}}{\partial t} + \rho_{\mathrm{f}} c_{p,\mathrm{f}} \vec{u} \cdot \nabla T_{\mathrm{f}} = \nabla \cdot \left(k_{\mathrm{f}} \nabla T_{\mathrm{f}} \right) - \rho_{\mathrm{f}} L \frac{\partial f}{\partial t} \tag{4}$$

6

where ρ and β were density and thermal expansion coefficient; where the coefficient A was given by:

$$A = \frac{C(1-f)^2}{S+f^3} \tag{5}$$

where C is the mushy zone parameter; S is a small constant to avoid the discontinuity; and f is the melting fraction in the PCM.

For heat transfer in metal foams, the energy transport can be governed by:

$$\rho_s c_{p,s} \frac{\partial T_s}{\partial t} = \nabla \cdot (k_s \nabla T_s) \tag{6}$$

Finally, the conjugate heat transfer between PCM and metal foam surface can be governed by:

$$T_s = T_f , \; k_s \frac{\partial T_s}{\partial n} = k_f \frac{\partial T_f}{\partial n} \tag{7}$$

where k, c_p, T and L are the thermal conductivity, specific heat, temperature and latent heat, respectively. The subscripts f and s represent PCM and metal foam, respectively.

2.4. Experimental uncertainty analysis

The experimental uncertainties mainly include the temperature measured by thermocouples and infrared camera, the volume of paraffin, the size of the 3D printed metal foam and the housing. For the temperature measurement system using Omega T-type thermocouples connected to the Agilent 34972A data log, the uncertainty δT_{TC} is ± 0.5 °C. The uncertainty δT_{inf} of the temperature measured by the infrared camera is ± 0.7 °C. The uncertainty δS_{3D} of 3D printed is mainly caused by the processing and measurement uncertainty, which is estimated to be less than 0.05 mm. The uncertainty δS_{ple} of the plexiglass size and δS_p of paraffin volume are mainly caused by the measurement, and both are estimated to be 0.1 mm. It was estimated that the uncertainty of the current test was 3.7% by Eq. (8) [34].

$$U = \sqrt{\left(\frac{\delta T_{TC}}{T_{TC}}\right)^2 + \left(\frac{\delta T_{inf}}{T_{inf}}\right)^2 + \left(\frac{\delta S_{3D}}{S_{3D}}\right)^2 + \left(\frac{\delta S_{ple}}{S_{ple}}\right)^2 + \left(\frac{\delta S_p}{S_p}\right)^2} \times 100\% \tag{8}$$

3. RESULTS AND DISCUSSIONS

3.1. Visualization experiment

3.1.1. Phase fields

Fig. 6(a) presents the phase images of the melting process for both pure PCM and case 1 observed from the top view. The white and transparent sections represent the solid and liquid paraffin, respectively. It can be observed from Fig. 6(a) that the translucent part implies the melting interface and the dashed lines shows the solid-liquid PCIs on phase images. The red dashed line represents the upper surface, while the yellow dashed line represents the bottom subface in terms of the transparency variation of paraffin.

For pure PCM, as shown in Fig. 6(a), a very thin piece of translucent paraffin can be observed at t = 40 s near wall A. Then the melting process can be clearly noticed at 100 s. Afterwards, the PCI gradually moved to wall C, which is almost parallel to wall A. Because of the uneven shape of the solid paraffin surface and the liquid paraffin flows into the pit, a local bending phenomenon can be found at t = 500 s. From t =500 s to t = 2000 s, the top and bottom PCI gradually moved to wall C, and the moving speed of the top PCI is faster than that of the bottom PCI. At t =2000 s, there is no solid paraffin at the upper surface of the pure PCM, while some solid paraffin can still be observed at the bottom subface. It means that the paraffin at the top melts faster than that at the bottom.

For case 1, at t = 40 s, the white paraffin that closes to wall A disappears and turns into translucent, which means that the melting process started to occur. From t = 100 s to t = 400 s, paraffin near wall A is completely melted, and the transparency of the overall paraffin increases, especially in the local area near the metal foam and wall A. However, this transformation remains insignificant in most regions of the foam pores. From t = 500 s to t = 700 s, more and more paraffin melts, and only a small portion of translucent paraffin is still close to wall C. In the pore area, the paraffin shows the concentric circles, and the closer to the center, the less transparent it is. After t = 1000 s, the solid paraffin is invisible from the top view, which indicates that the melting process is completed.

Comparing the phase felids of the pure PCM and composite PCM, the PCM of case 1 far from wall A melts earlier than pure PCM, which is attributed to that the metal foam is characterized by porous structures with large heat exchange area and the high thermal conductivity of the metal foam. The PCM of case 1 far away from wall A can indirectly and quickly absorb the heat from wall A through the metal foam, which improves the overall heat transfer performance of the composite PCM. In addition, the shape of the PCI of the pure PCM is relatively legible from the top view, which is mainly determined by the shape of the heating wall, and generally moves forward and parallel to the heating wall. However, the shape of the PCI for the composite PCM is affected by the metal foam. Finally, the melting process of the pure PCM completes at 2500 s, while case 1 finishes at 1000 s. The total melting speed of paraffin is increased by 2.5 times when 3D printed aluminum alloy metal foam with a porosity of 0.838 is applied.

3.1.2. Infrared temperature fields

The infrared temperature fields from the top view for both pure PCM and case 1 are given in Fig. 6 (b). The temperature distributions show the same behaviour as that for phase distributions. It can be observed that the temperatures on both sides of the PCI are significantly different. It indicates that the paraffin absorbs a large amount of latent heat during the phase change process with smaller temperature change.

For pure PCM, at the initial stage (from t = 40 s to t = 400 s) of the melting, the temperature of pure paraffin near wall A is higher than that at other locations due to low thermal conductivity of paraffin. Meanwhile, liquid paraffin temperature is much higher than the melting point due to the insulation of PCI, while solid PCM away from wall A has a very little temperature change. In Fig. 6 (a), at t = 500 s, it can be observed that the same temperature distribution of the local protrusions is achieved due to the physical shape of the solid paraffin. After that, the isotherm gradually moves towards wall C until the temperature of the surface exceeds the melting point temperature. At this moment, the top PCM melting is completed and the temperature distribution is almost kept the same.

For case 1, from t = 40 s to t = 400 s, the temperature of the PCM near wall A reaches the phase transition temperature. For the vast difference in thermal diffusivity between the metal foam and PCM, it can be noted that the temperature of the metal foam is higher than that of the nearby PCM, and the metal foam frame gradually appears. It means that there is a temperature difference between the metal foam and PCM. From t = 500 s to t = 700 s, the temperature of the central region gradually reaches the phase transformation temperature. The paraffin that is closest to the metal foam frame will melt first while the paraffin temperature in the center of the metal foam pores is the lowest due to small thermal diffusivity for paraffin. The temperature regions are distributed in the form of concentric circles, as shown in yellow ellipses in Fig. 6(b). The circle's size gradually increases from wall B to wall D since only wall B is insulated. At t = 800 s, the temperature of the central area exceeded the melting point temperature. Then at t = 1000 s, the upper surface temperature exceeds the melting point temperature. The thermal conductivity of the metal foam is

much greater than that of paraffin, the temperature of the metal foam on the surface is significantly lower.

Comparing the temperature fields of pure PCM with that for case 1, it can be observed clearly that the temperature distribution of the composite PCM is affected by the metal foam, and the shape is more complicated. The temperature difference of the composite PCM is much smaller than that of pure PCM, the biggest temperature difference of the composite PCM is about 10 °C at t = 400 s, which is smaller than that of pure paraffin at 30°C when t = 400 s. The composite PCM heat transfer performance shows better performance and the temperature distribution is more uniform.
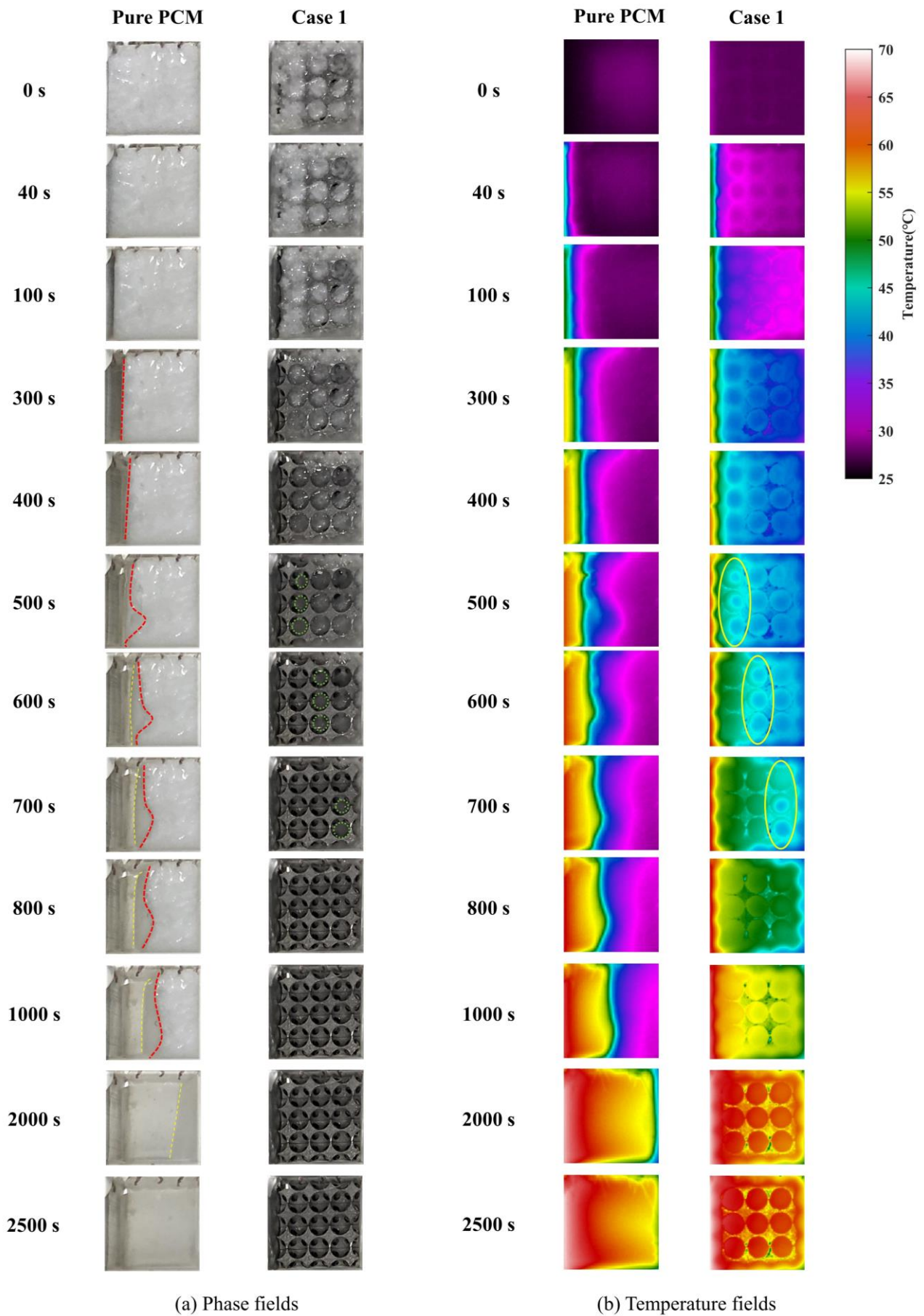
(a) Phase fields

(b) Temperature fields

Fig. 6. Phase and infrared temperature fields for pure PCM and case 1 (top view).

3.2. Effect of natural convection

Figs. 7 and 8 demonstrate the front view phase images for pure PCM and case 1. For pure PCM at t = 500 s, the PCI shows a central protrusion curve. Since wall A heats the bottom plexiglass while heating the PCM, the paraffin at the bottom starts to melt earlier than that at the center. In addition, the melted paraffin absorbs the heat from the heating surface and its density decreases and tends to move upwards. Subsequently, the top high temperature liquid paraffin flows downward and exchanges the heat with the solid PCM near the top PCI. At t = 1000 s, the PCI tilts to wall C due to the clockwise natural convection of liquid paraffin. As the liquid PCM increases, the natural convection is strengthened and the melting speed of PCM at the top is accelerated, thus, the bottom PCM melting speed becomes relatively slow. After t = 1000 s, the PCI continues to move to wall C. The whole pure PCM has been covered with the liquid paraffin at t = 2000 s and no more solid paraffin at 2500 s.

For case 1, from t = 500 s to t = 700 s, it can be observed that the shape of the PCI is completely affected by the metal foam. The closer to the metal foam, the more transparent the PCM is. At t = 800 s, the paraffin almost melts into liquid state, except for the little solid paraffin in the upper right corner for the cooler external environment. However, the PCM close to the bottom absorbs the heat from both bottom metal and the plexiglass, and it melts faster than that at the top. Appling similar PPI and porosity composite PCM made by conventional methods, Li et al. [3] observed similar melting processes and heat transfer performance.

There is no obvious sloped PCI shape during the melting process of composite PCM. The right corner PCM melting hysteresis in pure PCM is also improved. The effect of natural convection on the composite PCM is weakened, which means that the metal foam inhibited the natural convection. However, the phase change rate of the composite PCM is effectively improved, indicating that the metal foam's suppression on the natural convection of the liquid PCM is less than its enhancement effect on the heat conduction of the composite PCM.
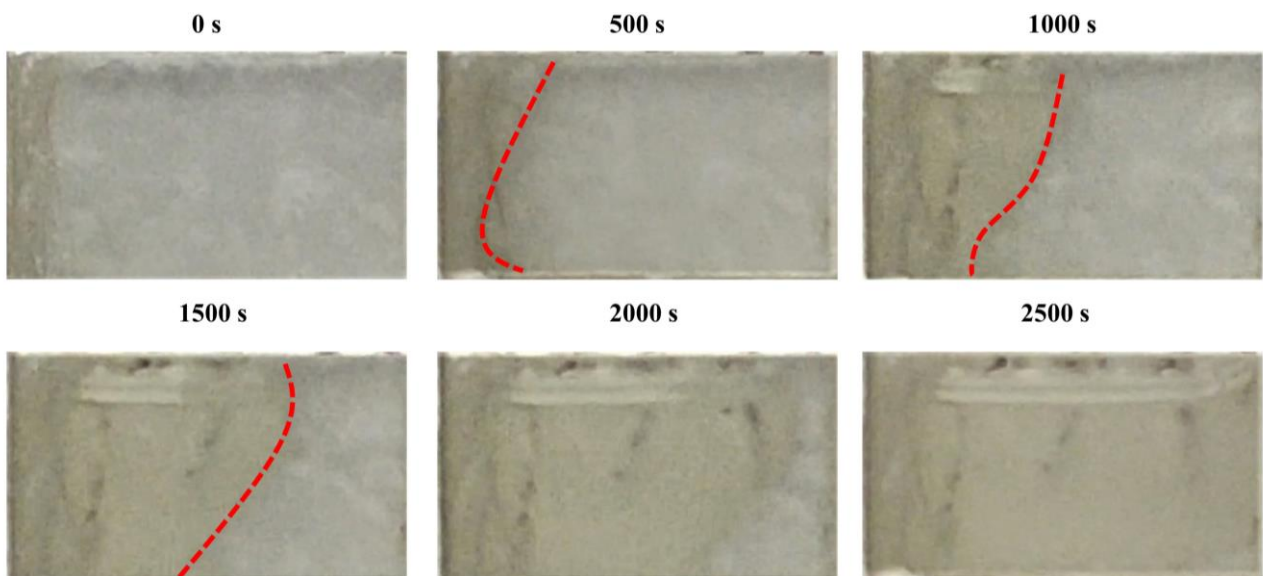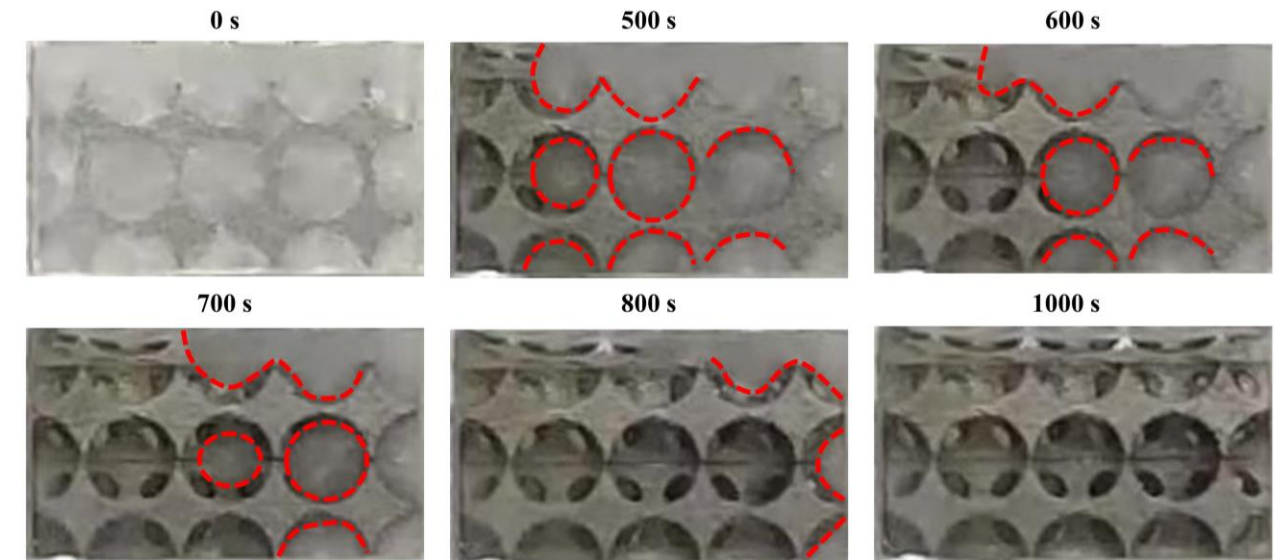

Fig. 7. Phase fields of pure PCM (front view).

Fig. 8. Phase fields of case 1 (front view).

3.3. Effect of the contact thermal resistance

It is impossible to avoid the contact thermal resistance between the different properties of the metal foam, which will certainly hinder the effect on the heat transfer process of the composite PCM. Fig. 9 displays the phase fields from the top view for case 2 and the corresponding temperature fields are shown in Fig. 10.

Compared with Fig. 6 (a) (from t = 100 s to t = 400 s), there is no overall transparency increase in Fig. 9. However, there is still a little of solid paraffin at wall B, wall C and wall D at 1000 s, which means the contact thermal resistance between the metal foams hinders heat transfer. Wall D remains more solid PCM than that at wall B from t = 400 s to t = 1000 s, which shows the effect of reducing heat dissipation for the insulation of wall B.
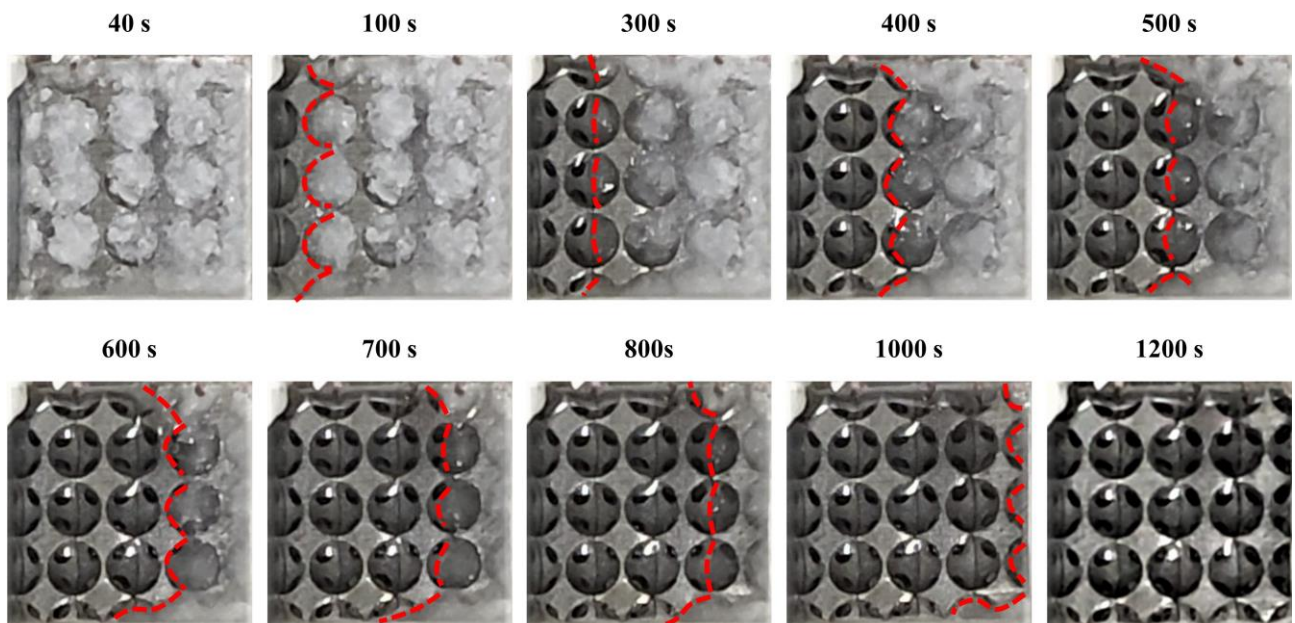

Fig. 9. Phase fields of case 2 (top view).

As depicted in Fig. 10, the temperature distribution of case 2 has a more obvious demarcation during the melting process. In addition, there are no concentric circles of temperature distribution

12

phenomenon as shown in Fig. 6 (b). It means that heat transfer is impeded by the contact thermal resistance between the metal foams. By comparing case 2 and case 1, the contact thermal resistance has a remarkable influence on the heat transfer process. The contact thermal resistance perpendicular to the heating direction hinders the heat transfer and slows down the phase change process.
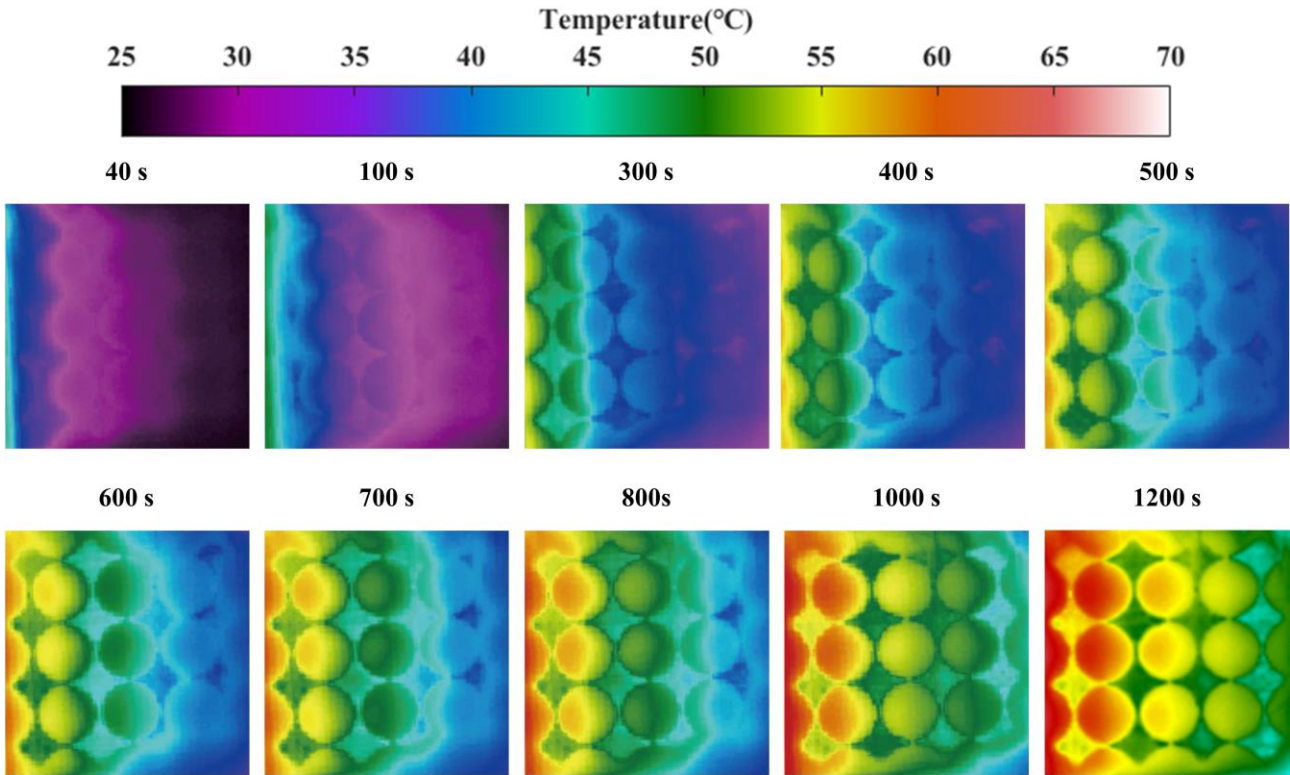

Fig. 10. Infrared temperature fields of case 2 (top view).

3.4. Time-temperature profile

The temperature profile for the pure PCM is plotted in Fig. 11. The temperature of the thermocouples placed at wall B is influenced by the heat dissipation of the wall and the temperature trends can be accepted for analysis. At t = 20 s, the temperature measured at the $T_{2,p}$ rise, while the temperatures at $T_{3,p}$, $T_{4,p}$ and $T_{5,\,p}$ rise at 40 s, 60 s and 160 s. Then, the paraffin has a slow temperature rise before its completion of melting, and it can be attributed to the low thermal conductivity of the paraffin, which suppresses the rate of heat transfer through the solid part. Once the paraffin melts, there is a sudden rise in the temperature, benefiting from the liquid PCM is heated and expanded, and the high temperature fluid flows upward naturally. Due to different distances from the heat source, temperatures at these measure points will reach the melting point temperature successively. Afterwards, the temperatures rise rate slows down, winch implies that the heat exchange has gradually stabilized. After achieving the stabilization of heat exchange, the temperatures at the measurement points are lower than that of the heating surface since ideal adiabatic conditions cannot be established.

Fig. 12 and Fig. 13 show the comparison of temperature variation for both case 1 and case 2. It indicates that the thermal response rate of composite PCM can be significantly improved, compared with pure PCM. For case 1 at the initial stage, the temperature gradients of $T_{2,f1}$, $T_{3,f1}$, $T_{4,f1}$ and $T_{5,f1}$ are bigger than that of pure PCM. It means that the paraffin absorbs the heat quickly in composite PCM. The phase transition completion times of these measurement points are 475 s, 710 s, 855 s and 925 s, which are faster than that of pure PCM. It is depicted that 3D printed aluminum alloy

metal foam could actively improve the phase change rate of paraffin. In addition, the temperature behaviour shows the same tendency for both case 1 and case 2. It can be observed that the overall phase transition time is delayed due to the contact thermal resistance between each column of metal foam.
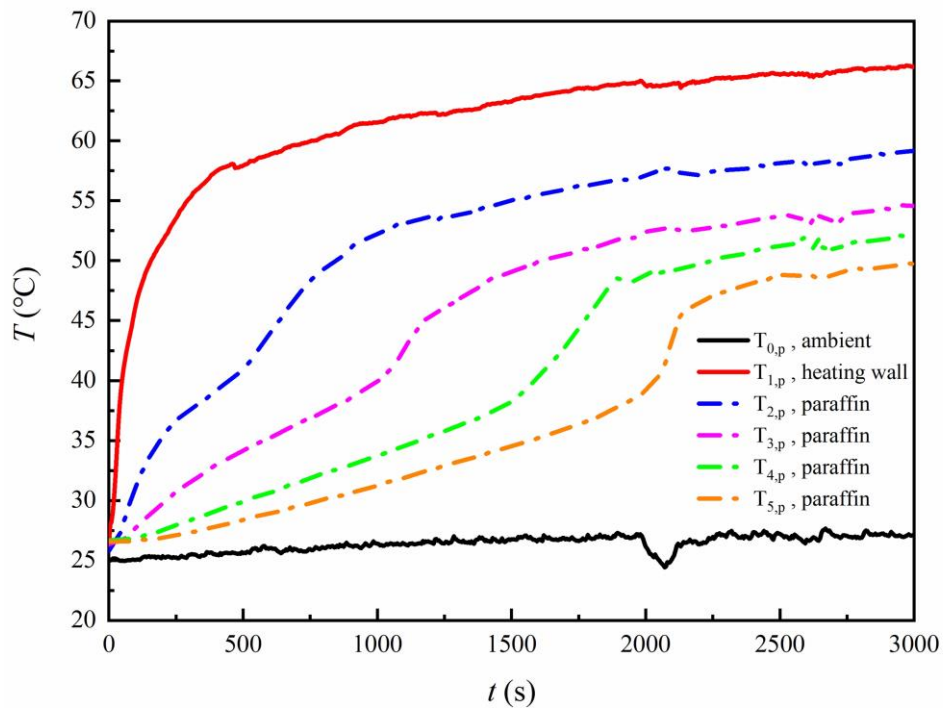

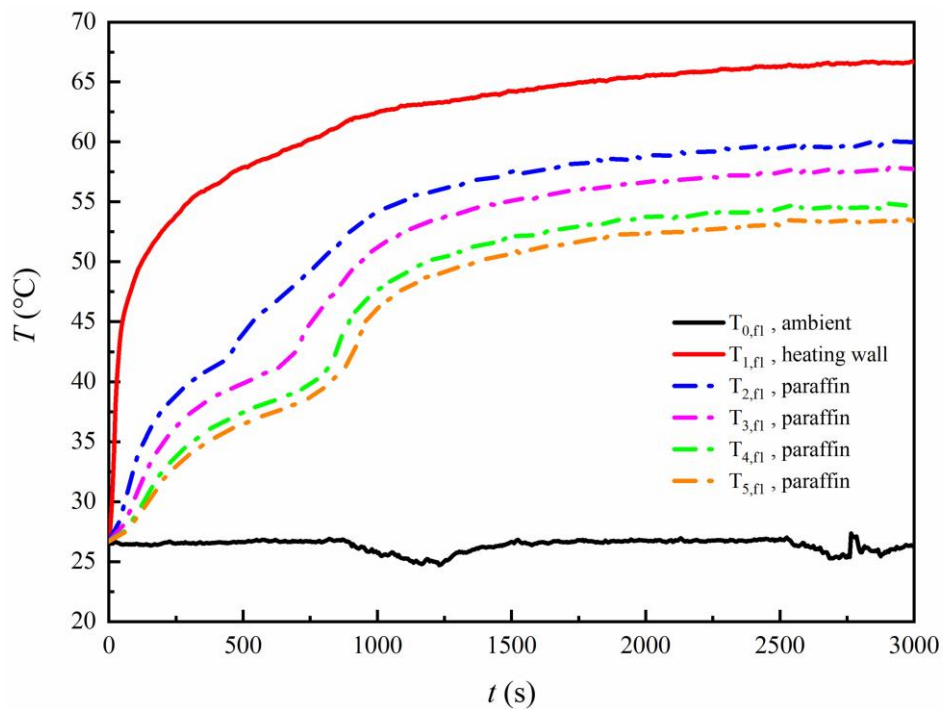**Fig. 11.** Temperature variations of pure PCM.

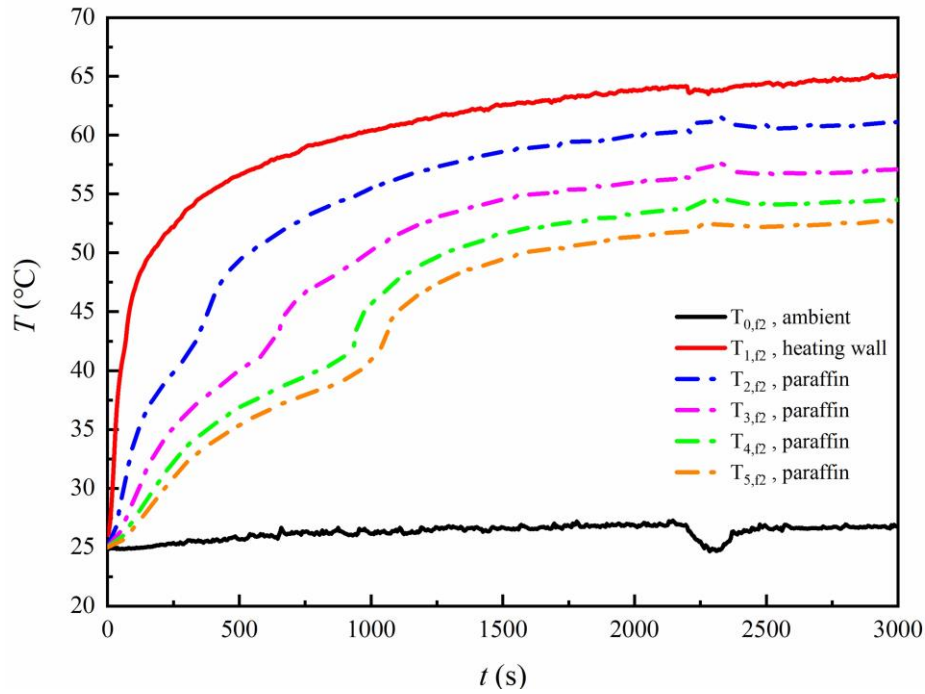**Fig. 12.** Temperature variations of case 1.

Fig. 13. Temperature variations of case 2.

3.5. Thermal non-equilibrium effect

Fig. 14 is the temperature contour figure at 400 s of case 1. The shape of the metal foam frame can be clearly observed in the Fig. 14. Fig. 15 shows the temperature variation along the Line 1 in Fig. 14. For the significant difference in thermal diffusivity between the paraffin and metal foam, the temperature exhibits periodic variation along the Line 1, which indicates that there exists significant effect of local thermal non-equilibrium between paraffin and 3D printed metal foam during melting process for case 1. The temperature difference ranges from 1 ℃ at 100 s to 2℃ at 400 s. In the later stages of the melting process, under the action of natural convection and lower thermal conductivity of PCM, the liquid PCM with higher temperature flows to the top and its downward circulation process is blocked by the metal foam frame, which makes the liquid PCM with higher temperature gradually gather at the top. As a result, the temperature of PCM on line 1 is obviously higher than that of foam metal. It is necessary to consider the local thermal non-equilibrium effect when developing the metal foam structure to accurately analyse the melting performance for composite PCM.
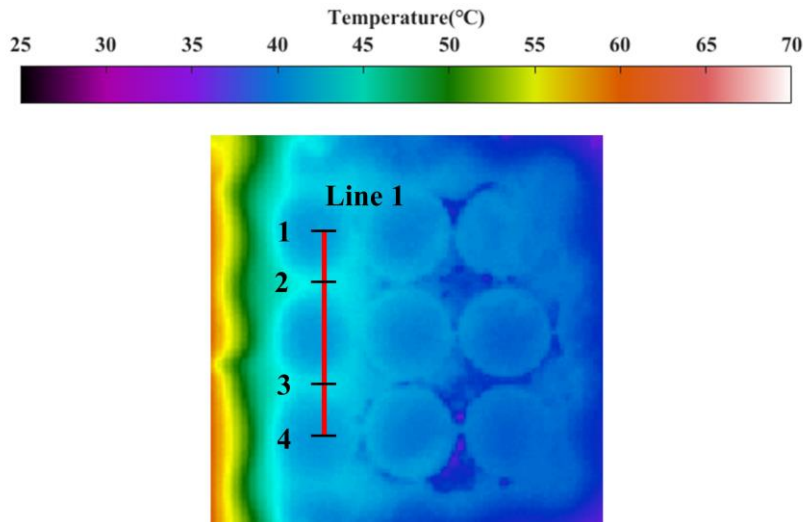

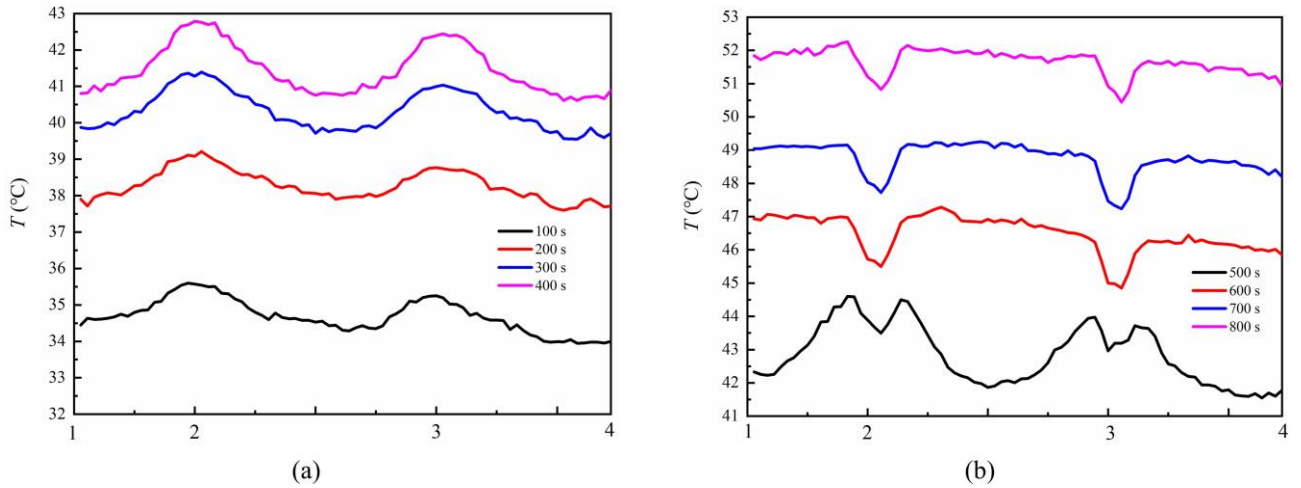**Fig. 14.** Temperature contour at 400 s of case 1

Fig. 15. Temperature distribution on line 1: (a) from t = 100 s to 400 s; (b) from t = 500 s to 800 s

3.6 Thermal performance comparison

In order to quantitatively compare the thermal performance, the energy storage power was introduced [35] and defined as the ratio of the heat storage capacity to the complete melting time. The energy storage powers of three operating cases studied in this paper were shown in Table 3. The energy storage power of the composite PCMs is much higher than that of the pure PCM. Therefore, the 3D printed metal foam can increase the heat transfer rate of composite PCMs. In addition, the energy storage power of case 1 is slightly higher than that of case 2, which indicates the contact thermal resistance parallel to the heating surface plays a certain obstructive role in heat transfer.

Table 3 The energy storage powers of all cases.

	Pure PCM	Case 1	Case 2
Energy storage power (W)	0.36	0.71	0.63

4. CONCLUSIONS

This paper proposed a new composite PCM based on 3D printed technology. The melting processes of pure PCM and composite PCM were compared. The phase and temperature fields were obtained and analyzed. The major findings of the current study are as follows:

(1) The 3D printed metal foam can effectively enhance the phase change rate of PCM. When 3D printed ALSI10MG aluminum alloy metal foam with a porosity of 0.838 is employed, the melting rate of paraffin could be increased by 2.5 times.
(2) The phase and temperature fields in the composite PCM are affected by the 3D printed metal foam, and the shape is highly similar to the 3D printed foam aluminum alloy. The temperature field is more uniform in composite PCM.
(3) The utilization of 3D printed metal foam hinders the natural convection of PCM and enhances thermal conductivity. In terms of the heat transfer performance, the 3D printed metal foam could improve the overall heat transfer performance of composite PCM.
(4) The contact thermal resistance between metal foams could directly affect the heat transfer efficiency of composite PCM.

16

(5) The local thermal non-equilibrium effects need to be considered between the metal foam and the PCM.

NOMENCLATURE

a	The side length of the cube	[m]
b	Diameter of removed ball	[m]
c_p	Specific heat	[J kg^{-1} K^{-1}]
f	Melting fraction	
k	Thermal conductivity	[W m K^{-1}]
L	Latent heat	[KJ kg^{-1}]
T	Temperature	[°C]
T_m	Melting temperature	[°C]
t	Time	[s]
U	Uncertainty	
V	Volume	[m^3]

Greek symbols

ε	Porosity	
μ	Dynamic viscosity	[Pa s]
ρ	Density	[kg m^{-3}]
β	Thermal expansion coefficient	[K^{-1}]
λ	Thermal conductivity	[W m K^{-1}]

Subscripts

f	PCM
f1	Case 1
f2	Case 2
inf	Infrared camera
p	Pure PCM
ple	Plexiglass
s	Metal foam
TC	Thermocouple
tot	Total volume

Acronyms

HD	High-definition
NEPCM	Nano-encapsulated PCM
PCM	Phase change material
PCI	Phase change interface
PPI	Pores per inch
SLM	Selective laser melting
3D	Three-dimensional

REFERENCES

[1] B. Mohammad Olfat, F. Talati. The effects of fins number and bypassed energy fraction on the solidification process of a phase change material. Journal of Energy Storage, 2021, 42: 102957.
[2] B. Fekadu, M. Assaye. Enhancement of phase change materials melting performance in a rectangular enclosure under different inclination angle of fins. Case Studies in Thermal Engineering, 2021, 25: 100968.

[3] H. Li, C. Hu, Y. He, et al. Visualized-experimental investigation on the energy storage performance of PCM infiltrated in the metal foam with varying pore densities. Energy, 2021, 237: 121540.

[4] G. K. Marri, C. Balaji. Experimental and numerical investigations on the effect of porosity and PPI gradients of metal foams on the thermal performance of a composite phase change material heat sink. International Journal of Heat and Mass Transfer, 2021, 164: 120454.

[5] S. Sami, N. Etesami. Heat transfer enhancement of microencapsulated phase change material by addition of nanoparticles for a latent heat thermal energy storage system. Energy Reports, 2021, 7: 4930-4940.

[6] G. K. Amudhalapalli, J. K. Devanuri. Synthesis, characterization, thermophysical properties, stability and applications of nanoparticle enhanced phase change materials – A comprehensive review. Thermal Science and Engineering Progress, 2021: 101049.

[7] M. Ren, Y. Liu, X. Gao. Incorporation of phase change material and carbon nanofibers into lightweight aggregate concrete for thermal energy regulation in buildings. Energy, 2020, 197: 117262.

[8] Y. Cui, C. Liu, S. Hu, et al. The experimental exploration of carbon nanofiber and carbon nanotube additives on thermal behavior of phase change materials. Solar Energy Materials and Solar Cells, 2011, 95(4): 1208-1212.

[9] Y. Yao, H. Wu, Z. Liu, et al. Pore-scale visualization and measurement of paraffin melting in high porosity open-cell copper foam. International Journal of Thermal Sciences, 2018, 123: 73-85.

[10] Y. Yao, H. Wu, Z. Gao, et al. Pore-scale visualization and measurement of paraffin solidification in high porosity open-cell copper foam. International Journal of Thermal Sciences, 2019, 135: 94-103.

[11] W. Li, S. Guo, L. Tan, et al. Heat transfer enhancement of nano-encapsulated phase change material (NEPCM) using metal foam for thermal energy storage. International Journal of Heat and Mass Transfer, 2021, 166: 120737.

[12] S. Feng, Y. Zhang, M. Shi, et al. Unidirectional freezing of phase change materials saturated in open-cell metal foams. Applied Thermal Engineering, 2015, 88: 315-321.

[13] S. Mancin, A. Diani, L. Doretti, et al. Experimental analysis of phase change phenomenon of paraffin waxes embedded in copper foams. International Journal of Thermal Sciences, 2015, 90: 79-89.

[14] W. Tian, S. Dang, G. Liu, et al. Thermal transport in phase change materials embedded in metal foam: evaluation on inclination configuration. Journal of Energy Storage, 2021, 33: 102166.

[15] M. Caliano, N. Bianco, G. Graditi, et al. Analysis of a phase change material-based unit and of an aluminum foam/phase change material composite-based unit for cold thermal energy storage by numerical simulation. Applied Energy, 2019, 256: 113921.

[16] A. Siahpush, J. O'Brien, J. Crepeau. Phase Change Heat Transfer Enhancement Using Copper Porous Foam. Journal of Heat Transfer, 2008, 130(8): 318-323.

[17] A. Diani, M. Campanale. Transient melting of paraffin waxes embedded in aluminum foams: Experimental results and modeling. International Journal of Thermal Sciences, 2019, 144: 119-128.

[18] X. Hu, X. Gong. Pore-scale numerical simulation of the thermal performance for phase change material embedded in metal foam with cubic periodic cell structure. Applied Thermal Engineering, 2019, 151: 231-239.

[19] X. Yang, S. Feng, Q. Zhang, et al. The role of porous metal foam on the unidirectional solidification of saturating fluid for cold storage. Applied Energy, 2017, 194: 508-521.

[20] Z. Zhang, X. He. Three-dimensional numerical study on solid-liquid phase change within open-celled aluminum foam with porosity gradient. Applied Thermal Engineering, 2017, 113: 298-308.

[21] C. Hu, H. Li, D. Tang, et al. Pore-scale investigation on the heat-storage characteristics of phase change material in graded copper foam. Applied Thermal Engineering, 2020, 178: 115609.

[22] X. Li, J. Duan, T. Simon, et al. Nonuniform metal foam design and pore-scale analysis of a tilted composite phase change material system for photovoltaics thermal management. Applied Energy, 2021, 298: 117203.

[23] S. Feng, M. Shi, Y. Li, et al. Pore-scale and volume-averaged numerical simulations of melting phase change heat transfer in finned metal foam. International Journal of Heat and Mass Transfer, 2015, 90: 838-847.

[24] J. R. McDonough. A perspective on the current and future roles of 3D printed technology in process engineering, with an emphasis on heat transfer. Thermal Science and Engineering Progress, 2020, 19: 100594.

[25] D. Jafari, W. W. Wits, B. J. Geurts. Metal 3D-printed wick structures for heat pipe application: Capillary performance analysis. Applied Thermal Engineering, 2018, 143: 403-414.

[26] D. A. Ramirez, L. E. Murr, S. J. Li, et al. Open-cellular copper structures fabricated by 3D printed technology using electron beam melting. Materials Science and Engineering: A, 2011, 528(16-17): 5379-5386.

[27] L. Fratalocchi, G. Groppi, C. G. Visconti, et al. Adoption of 3D printed highly conductive periodic open cellular structures as an effective solution to enhance the heat transfer performances of compact Fischer-Tropsch fixed-bed reactors. Chemical Engineering Journal, 2020, 386: 123988.

[28] D. A. Ramirez, L. E. Murr, S. J. Li, et al. Open-cellular copper structures fabricated by 3D printed technology using electron beam melting. Materials Science and Engineering: A, 2011, 528(16-17): 5379-5386.

[29] S. J. Li, Q. S. Xu, Z. Wang, et al. Influence of cell shape on mechanical properties of Ti-6Al-4V meshes fabricated by electron beam melting method. Acta Biomater, 2014, 10(10): 4537-4547.

[30] S. L. Sing, F. E. Wiria, W. Y. Yeong. Selective laser melting of lattice structures: A statistical approach to manufacturability and mechanical behavior. Robotics and Computer-Integrated Manufacturing, 2018, 49: 170-180.

[31] Z. Hu, D. Wang, J. Xu, et al. Development of a loop heat pipe with the 3D printed stainless steel wick in the application of thermal management. International Journal of Heat and Mass Transfer, 2020, 161: 120258.

[32] Z. A. Qureshi, E. Elnajjar, O. Al-Ketan, et al. Heat transfer performance of a finned metal foam-phase change material (FMF-PCM) system incorporating triply periodic minimal surfaces (TPMS). International Journal of Heat and Mass Transfer, 2021, 170: 121001.

[33] K. B. Saleem, K. Ghachem, L. Koufi, et al. Analysis of Double-diffusive natural convection in a solar distiller embedded with PCM and cooled with external water stream. Journal of the Taiwan Institute of Chemical Engineers, 2021, 126: 67-79.

[34] C. Zhao, W. Lu, Y. Tian. Heat transfer enhancement for thermal energy storage using metal foams embedded within phase change materials (PCMs). Solar Energy, 2010, 84(8): 1402-1412.

[35] H. Li, C. Hu, Y. He, et al. Visualized-experimental investigation on the energy storage performance of PCM infiltrated in the metal foam with varying pore densities. Energy, 2021, 237: 121540.